Indian Journal of Pure & Applied Physics
Vol. 59, January 2021, pp. 11-22

A Combined Experimental and first principle studies on $(ZnO)_{12}$ nanocluster

S Dheivamalar[a*] & K Bansura banu[a,b]

[a] PG & Research Department of Physics, Periyar E V R College (Autonomous), Tiruchirappalli-620 023, India

[b] PG & Research Department of Physics, Holy Cross College (Autonomous), Tiruchirappalli-620002, India

Received 24 December 2019; accepted 4 December 2020

We report the biogenic synthesis of ZnO nanoparticles using *Mangifera indica* aqueous extract and density functional theory/time-dependent density functional theory (DFT/TD-DFT) calculations on $Zn_{12}O_{12}$ nanocluster compared with various basis sets (B3LYP/6-31G, B3LYP/LANL2DZ, and B97D). The genesis of ZnO nanoparticles was achieved from the reduction of capping agent $ZnSo_4$. The properties of ZnO nanoparticles were signalized by UV, FTIR, FESEM-EDAX, and XRD analysis. The intense band at 380nm in the UV-Vis absorption spectrum results from the formation of ZnO nanoparticles. The structure of ZnO nanoparticles was anatomized by FESEM analysis and the presence of Zn was confirmed using EDAX. The frontier molecular orbital exploration has been investigated to govern the charge transfer characteristics of donor-acceptor moieties of the $Zn_{12}O_{12}$. The energy gap (Eg), binding energy (E_B), global reactivity descriptors, and the total dipole moment has also been investigated for $Zn_{12}O_{12}$. The total density of states (DOS) was analyzed to describe the orbital hybridization of $Zn_{12}O_{12}$. Mulliken atomic charge distribution, NBO analysis and molecular electrostatic potential (MEP) have also been studied. The first-order hyperpolarizability calculation proves that the $Zn_{12}O_{12}$ is a suitable candidate with the predominant nonlinear optical property. TD-DFT excited state analysis of $Zn_{12}O_{12}$ was completely consistent with the experimental data of the UV-Vis spectrum makes its application in solar cells.

Keywords: Nano cluster, $Zn_{12}O_{12,}$ Density of states, Density functional theory.

1 Introduction

Nano structured materials of II-VI and III-V semiconductors in modern sciences are currently of great interest due to their reduced dimensions and are majorly taking part in a dye-sensitized solar cell devices. The ZnO nanostructured materials are of greater importance owing to their nano morphology, nontoxicity, functionality, and biocompatibility[1-3]. The ZnO nanoparticles have gained the major attention of researchers due to their novel properties and probable applications in piezoelectric devices, UV absorbers, sensors, pharmaceuticals, and cosmetic industries[4,5]. The ZnO nanostructured material has an immense band gap which makes this material as the best semiconductor with the highest excitation binding energy in addition to low lasting threshold[6,7]. The developments of ZnO nano structured materials have been growing exponentially in the ended handful years, which were proven by numerous experimental and theoretical studies of ZnO related papers in the literature. The semiconductor ceramic compound ZnO exhibits good electrical conductivity and transmittance[8]. ZnO nanomaterial has pertinence in solar cells[9] gas sensors[10] piezoelectric materials[11] and electrodes[12]. The relative affluence of $(ZnO)_{11}$, $(ZnO)_{12}$ and $(ZnO)_{13}$ nanoclusters were majorly studied by Behran *et al.*[13]. The optoelectronic behavior of hexagonal structured ZnO nanocluster was analyzed by Malloci *et al.*[14]. The experimental observation of ZnO nanoparticles has been envisioned by Masuda *et al.*[15]. Among all these, fewer considerations have been adopted to correlate the experimental and theoretical observations of ZnO nanocluster. The preparation of ZnO nanomaerials was achieved through various synthesis techniques, namely sol-gel[16], hydrothermal[17], micro-wave assisted synthesis[18], micro-emulsion[19], chemical vapour deposition[20], vapour phase transport[21], homogeneous precipitation[22], direct precipitation[23], mechanochemical[24], spray pyrolysis[25] thermal decomposition[26] and radio frequency plasma[27]. Among all, the biogenic synthesis is the promising method to produce advanced functional nano particles. The biogenic synthesis is one the cleanest, biocompatible, non-toxic and eco-friendly methods through large-scale production[28]. *Mangifera Indica* well known as Mango that has been commonly used as a herb in ayurvedic medicine. The wide ranging survey of literature communicated that

*Corresponding author (E-mail: sitrulinsiragugal@gmail.com)

the Mangifera indica is an important source of many pharmacological and medicinally important chemicals such as mangiferin, mangiferonic acid, hydroxyl mangiferin, polyphenols and carotenes[29-31].

The *Mangifera* plant possesses anti diabetic, antioxidant, antiviral, anti allergenic, cardiotonic, hypotensive, anti inflammatory, anti parasitic properties. The ZnO nanoparticles synthesized from Mangifera indica possessed many noteworthy biological roles as drug delivery, food production, agriculture, diagnostics and treatment[32]**.** The objective of the present investigation is the biogenic synthesis of ZnO nanoparticles form *Mangifera indica* plant extract *via* sulphate route with quantum chemical calculations of $Zn_{12}O_{12}$ nanocluster using DFT/TD-DFT methods for the first time. To date, as per authors knowledge there is no report of DFT/TD-DFT computations of $Zn_{12}O_{12}$ cluster with different basis sets and their optical, electrical and structural properties are compared with the ZnO nanoparticles synthesized from *Mangifera indica* plant extract. The green synthesized ZnO nanoparticles were examined by surface morphology, structure and spectral analysis. Simulated UV spectra, FTIR spectrum geometry optimization of $Zn_{12}O_{12}$ were studied and compared with experimental XRD and UV-Vis spectrum and FTIR spectral data. This paper focuses how the experimental and first principle simulations favored the formation of a stable cluster of $Zn_{12}O_{12}$ for dye sensitized solar cell applications owing to their higher photon to current conversion efficiency, low cost and ease of fabrication. The conduction band LUMO of $Zn_{12}O_{12}$ is higher energy that causes sufficient electron injection and conduction band HOMO of $Zn_{12}O_{12}$ is lower energy to accept the electrons makes its application in dye sensitized solar cells.

2 Experimental

2.1 Materials

Zinc Sulphate ($ZnSo_4$) and anhydrous ethanol (C_2H_5OH) were guaranteed reagents of Precision scientific companies, all of analytical purity were used for the preparation of Zno nanoparticles. The plant leaves of *Mangifera indica* were collected from the campus of Tiruchirappalli, India. The glass wares used in the experiments were cleaned with chromic acid followed by thorough washing with distilled water.

2.2 Preparation of Leaf Extract:

The collected plant leaves of *Mangifera indica* were cleaned under running tap water followed by double deionized water. The leaves were dried under theshadow at room temperature and then weighed 30gm of the dried leaves and cut them into small pieces using a sharp knife. The small pieces of leaves were boiled in 300 ml of double deionized water at 50 ºC in magnetic stirrer for 1hr 45min. The boiled mixture was cooled at room temperature and filtered through Whatman No.1 filter paper (pore size 25 μm). Now the plant extracts are ready to use and stored at 4 ºC for further use.

2.3 Synthesis of ZnO nanoparticles

The cell filtrate of *Mangifera indica* was used for the production of ZnO nanoparticles. 50 ml of the filtered *Mangifera indica* extract was used to dissolve in Zinc sulfate without any additional heat treatment. The mixture is covered with foil to avoid any photoinduced phenomenon and kept at room temperature. Yet there was an obvious colour change after 18h, but no precipitate suggesting that any information of a Zinc complex was in the form of a suspension. The precipitate was dried in an oven at 100 °C and ground to a fine powder using agate mortar and washed several times with ethanol and deionized-H_2O to remove any residue of the extract. The powder obtained from the above method was calcinated at different temperatures such as 200, 300 400, 600, and 800 °C for 2h. This ZnO nanoparticle was characterized using UV, FESEM, EDAX, FTIR and XRD analysis.

2.2 Computational methods:

Geometry optimization of $Zn_{12}O_{12}$ cluster was carried out using the framework of the density functional theory (DFT) method. The hybrid density functional B3LYP and correlation functional of Lee-Yang- Parr with B3LYP/6-31G, M06-L, B3LYP/LANL2DZ and B97D basis sets are used to obtain a better approximation to demonstrate the energy of highest occupied molecular orbital (E_{HOMO}), the energy of lowest unoccupied molecular orbital (E_{LUMO}) and the energy difference between them as energy gap ($E_g = E_{LUMO} - E_{HOMO}$) for $Zn_{12}O_{12}$ in Gaussian 09 suites of program[33,34]**.** The electronic states for the lower spin as a singlet state (spin multiplicity = 1) were applied. The density of states (DOS) for $Zn_{12}O_{12}$ nanostructure was plotted by employing Gauss Sum Program[35]**.** The calculation of the dipole moment, chemical parameters, thermodynamic parameters, vibrational frequencies, and polarizability were employed by B3LYP/6-31G

level of theory in Gaussian 09 program[36]. In further, molecular electrostatic potential (MEP) analysis and Mulliken charge distribution of each atom in the $Zn_{12}O_{12}$ were also implemented in the Gaussian 09 program. The TD-DFT computations were employed to evaluate the excitation energy, UV-Vis electronic transition, and oscillator strength of $Zn_{12}O_{12}$ cluster at TD-DFT computation with CAM-B3LYP/6-31G level and CIS method. The interaction between Zn and O atoms in $Zn_{12}O_{12}$ cluster can be achieved by the calculation of binding energy as:

$$E_B = E_{Zn12O12} - E_{Zn} - E_O \quad \ldots(1)$$

Where $E_{Zn12O12}$ is the total energy of $Zn_{12}O_{12}$ cluster, E_{Zn} is the total energy of the isolated Zn atom and E_O is the total energy of the isolated O atom in the cluster[37]. The negative binding energy specifies the exothermic process[38].

The energy gap E_g is defined as:

$$E_g = E_{LUMO} - E_{HOMO} \quad \ldots(2)$$

Where, E_{HOMO} and E_{LUMO} are the energies of HOMO and LUMO, respectively.

3 Results and Discussion

3.1 Structures and stability

The optimized geometries of three isomeric structures of $Zn_{12}O_{12}$ nanocluster have been obtained using the Gaussian 09 program in the singlet ground state. Among all the structures, the properties of three-dimensional drum structured $Zn_{12}O_{12}$ have been scrutinized in this script is shown in Fig. 1. The mentioned variant is more significant because of this cluster size is that most known ZnO presentations are related to hexagonal forms and we expect that $Zn_{12}O_{12}$ nanocluster represents a superior potential source for

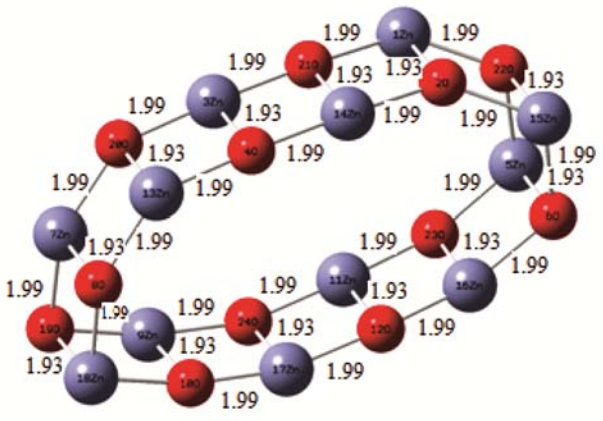

Fig. 1 — The optimized drum structure of $Zn_{12}O_{12}$ with bond distances calculated at B3LYP/6-31G level of theory.

further more research. The structural data from ground state analysis by DFT computation with B3LYP/6-31G, B3LYP/LANL2DZ, and B97D basis sets and excited state analysis by TD-DFT and CIS computations of $Zn_{12}O_{12}$ were presented in Table 1.

The optimized geometry of drum structured $Zn_{12}O_{12}$ cluster has two hexagonal rings and twelve tetragons in the singlet ground state. The symmetry of the cluster is C_1 point group symmetry. Two different types of Zn-O bond lengths are identified within the $Zn_{12}O_{12}$. The bond length 1.93 Å is shared between two hexagons and the other bond length 1.99 Å is shared between the tetragon and a hexagon in the DFT optimization of B3LYP/6-31G functional. This bond length prediction is good agreeing with the experimental values of Zn-O bond calculated by Birajdar *et al.*[39] and Seetawan *et al.*[40]. The Zn-O bond lengths of $Zn_{12}O_{12}$ cluster calculated by TD-DFT are 1.91Å-1.93Å similar to Wang *et al.*[41]. The charge transportation from the Zn atoms to the O atoms in $Zn_{12}O_{12}$ is mainly due to the ionic bond of Zn-O. The bond angle of tetragons and hexagons in the $Zn_{12}O_{12}$ cluster varies from 89° to 91°and 116° to 124°. The interaction between Zn atoms and O atoms of $Zn_{12}O_{12}$ nanocluster were studied by calculating the corresponding binding energy E_B as -6.52Kcal/Mol. This calculation reveals that there was exothermic interaction with negative binding energy. By repeating all the computations by B3LYP/6-31G, B97D, and B3LYP/LanL2DZ level of calculation, the bond length was larger than it was computed by B3LYP/6-31G. The structural parameter calculated by DFT is correlated with the experimental XRD analysis. Figure 2 shows the XRD pattern of ZnO nanoparticles. All diffraction peaks were indexed to ZnO with a hexagonal wurtzite structure. The appearance of weak diffraction peaks corresponding to the (100), (002), (102), (110), (021), (013), (112) and (021) planes of ZnO suggested the presence of some randomly oriented grains. There was strong and intense diffraction along the (101) plane. This was comparable with other ZnO nanostructures studied by Hossain *et al.* and Noh *et al.*[42,43] but in contrary to Bacaksiz *et al.* and Yilmaz *et al.*[44,45]. Thermal treatments at higher temperature promotes the formation of ZnO wurtzite structure, which is characterized by the three major peaks at 2θ = 32-37°. The temperature at 200-300°C, the cubic ZnO observed at 2θ = 39° and 2θ= 34°. The temperature greater than 300°C, the peaks corresponding to ZnO are observed, indicates that the synthesized ZnO has high purity. The mean crystallite size (D) was evaluated according

Table 1 — The calculated bond length of $Zn_{12}O_{12}$ in the ground state (Gnd) and excited state (Exc) analysis at DFT/TD-DFT method with different basis sets and experimental bond length calculated at XRD analysis. All values in (Å)?

	$Zn_6O_{6\ (Gnd)}$			$Zn_6O_{6\ (Exc)}$		experimental bond length
Bond distance	B3LYP/6-31G	B3LYP/LanL2DZ	B97D	TD-DFT	CIS	
Zn(1)-O(2)	1.93	1.94	1.96	1.91	1.92	1.97
Zn(1)-O(7)	1.99	2.01	2.04	1.93	1.93	1.97
Zn(1)-O(9)	1.99	2.01	2.03	1.93	1.93	1.97
O(2)-Zn(10)	1.99	2.01	2.04	1.93	1.93	1.97
O(2)-Zn(12)	1.99	2.01	2.04	1.93	1.94	1.97
Zn(3)-O(4)	1.93	1.95	1.96	1.91	1.92	1.97
Zn(3)-Zn(10)	2.38	2.43	2.46	2.35	2.35	-
Zn(3)-O(8)	1.99	2.02	2.04	1.93	1.93	1.97
Zn(3)-O(9)	1.98	1.99	2.04	193	1.93	1.97
O(4)-Zn(10)	1.99	2.02	2.05	1.93	1.94	1.97
O(4)-Zn(11)	1.99	2.02	2.05	1.94	1.94	1.97
Zn(5)-O(6)	1.93	1.94	1.96	1.91	1.92	1.97
Zn(5)-Zn(12)	2.42	2.44	2.47	2.41	2.42	-
Zn(5)-O(7)	1.99	2.02	2.05	1.94	1.94	1.97
Zn(5)-O(8)	1.99	2.02	2.05	1.93	1.94	1.97
O(6)-Zn(11)	1.98	2.02	2.05	1.93	1.94	1.97
O(6)-Zn(12)	1.98	2.02	2.04	1.93	1.94	1.97
Zn(10)-Zn(12)	2.39	2.43	2.47	2.37	2.37	-
Zn(10)-O(9)	1.93	1.94	1.97	1.91	1.92	1.97
Zn(11)-O(8)	1.93	1.94	1.96	1.91	1.92	1.97
Zn(12)-O(7)	1.93	1.95	1.97	1.91	1.91	1.97

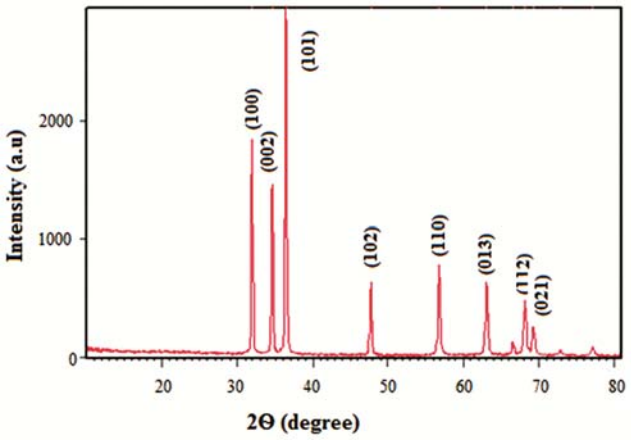

Fig. 2 — The XRD pattern of green synthesized ZnO nano particles.

to broadening of the highest intensity peak corresponding to the (101) diffraction plane using the Debye-Scherrer formula shown in Eq. (3)[46]

$$D=0.9\lambda/\beta\cos\theta \quad \ldots (3)$$

Where, λ, β, and θ are the X-ray wavelength (1.5418 Å), full width at half maximum (FWHM) in radians and Bragg's diffraction angle, respectively. The dislocation density (δ) was calculated from D using Eq. (4)[47]

$$\delta=1/D^2 \quad \ldots (4)$$

The value of D increases from 13 to 130 nm in the temperature range 200 to 800 °C. The dislocation density was found to be 1.7×10^{-3} nm^{-2}. This lower value for δ implied that our films had very few lattice defects and good crystalline qualities. The lattice parameters *a* and *c* were calculated using Eq. (5)[48]

$$1/d_{hkl}^2 =4/3(h^2 +hk+k^2/a^2) + l^2/c^2 \quad \ldots (5)$$

Where d_{hkl} is the interplanar spacing obtained from Bragg's law, and *h*, *k*, and *l* are the Miller indices denoting the plane.

The Zn-O bond length (L) was also calculated using Eqs. (6) & (7)[49]

$$L=\sqrt{(a^{2/3}+(1/2-u)^2\ c^2)} \quad \ldots (6)$$

$$u=a^2/3c^2+1/4 \quad \ldots (7)$$

Where, *u* is a wurtzite structure parameter. The calculated values of lattice parameters (Å), grain size (D) and bond length (Å) at different temperatures of ZnO nanoparticles using XRD analysis are listed in Table 2.

3.2 Frontier molecular orbital analysis

The π type molecular orbital characteristics are exhibited by the highest occupied molecular orbital

Table 2 — The calculated values of lattice parameters a, c (Å) and size D (nm) of ZnO nanoparticles using XRD analysis

Temperature °C	Lattice parameter *a* (Å)	Lattice Parameter *c* (Å)	Size *D* (nm)
200	3.256	5.237	13
300	3.251	5.221	24
400	3.253	5.215	31
600	3.254	5.2211	51
800	3.251	5.212	129

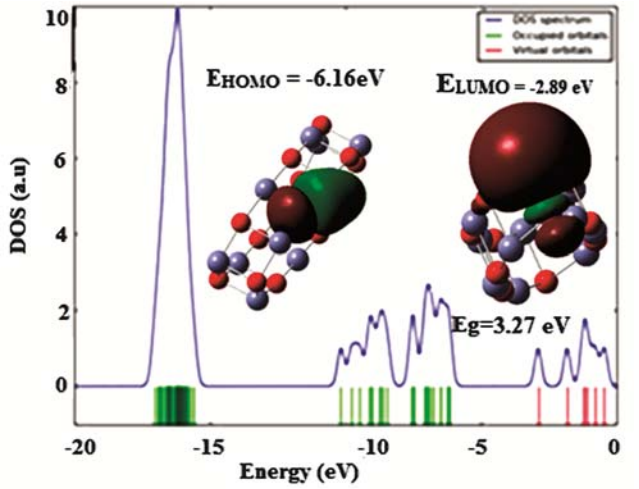

Fig. 3 — The HOMO/LUMO molecular orbitals of $Zn_{12}O_{12}$ nanocluster figured out at B3LYP/6-31G level of theory with DOS plot.

(HOMO) and the lowest unoccupied molecular orbital (LUMO) contours. The bonding behavior is specified by HOMO orbital and the antibonding features are enumerated by LUMO orbital. The $\pi - \pi^*$ transition correlated with the low lying singlet ground state. The HOMO/LUMO transition is identified as $\pi - \pi^*$ intramolecular interaction. The molecular interaction taking place between the HOMO which is an electron donor and the LUMO which is an electron acceptor is an index of kinetic stability[50]. Figure 3 shows the charge distribution of HOMO and LUMO of $Zn_{12}O_{12}$ computed by B3LYP/6-31G level of theory with DOS plot. The Zn atoms in the cluster have positive charge which are an acceptor and O atoms have negative charge which are the donor. It can be seen from Fig. 3, the positive region is shown in green color and the negative region is shown in red color. The HOMO levels are uniformly distributed in entire atoms in the $Zn_{12}O_{12}$ nanocluster. In the LUMO levels, green region is located over Zn atoms and the red region is sited on O atoms. The calculated energies of HOMO and LUMO for $Zn_{12}O_{12}$ using DOS are -6.16 and -2.89 eV with the band gap of 3.27 eV which is in good agreement with the maximum absorption of experimental UV-Vis absorption spectrum. The high energy gap of $Zn_{12}O_{12}$ cluster indicates more stable, high thermal stability and chemically inert towards reactivity. It specifies that the electron in the valence band requires more energy to go to the conduction band. The larger energy gap makes the nanocluster applied in electronic devices. Fermi level (E_F) in $Zn_{12}O_{12}$ cluster at (T=0 K) is roughly situated at the middle of the HOMO-LUMO energy gap (E_g) is -4.52 eV. The HOMO/LUMO energy, energy gap (E_g), adsorption energy (E_{ad}) and ΔE_g values of $Zn_{12}O_{12}$ calculated at different basis sets as B3LYP//6-31G, B3LYP/LANL2DZ, and B97D) were presented in Table 3.

The maximum open-circuit voltage (V_{oc}) of the solar cell relates the difference between the HOMO and the LUMO taking the energy lost during the photo charge generation. The theoretical values of V_{oc} are calculated from the following equation,

$$V_{oc} = \left| E_{HOMO}\,(\text{Donor}) \right| - \left| E_{LUMO}\,(\text{Acceptor}) \right| - 0.3 \quad \ldots (8)$$

An open-circuit voltage (V_{oc}) of 2.97 V cause the possible electron injection process and make the $Zn_{12}O_{12}$ nanocluster as a most efficient material in photovoltaic cells and its properties are optimal for the significant photovoltaic performance. The Energy gap E_g (3.27 eV) of $Zn_{12}O_{12}$ can harvest more light it assists the higher short-circuit current density (J_{sc}).

The short-circuit current density (J_{sc}) is closely connected to the charge conversion efficiency (η) of the solar cell is defined as:

$$J_{sc} = \int LHE\,(\lambda)\,\varphi_{Inject}.\eta_{collect}\,d\lambda \quad \ldots (9)$$

Where, LHE (λ) is the light harvesting efficiency, φ_{Inject} is the electron injection potency and $\eta_{collect}$ is the electron collection efficiency.

The large φ_{Inject} leads to higher short circuit current density (Jsc). The φ_{Inject} is analogous to the driving force of the electron inoculation (ΔG^{inject}) from the photoinduced excited state of A-$NiZn_6O_6$ on the semiconductor surface and φ_{Inject} is directly proportional to the free energy of electron injected as:

$$\varphi_{Inject}\,\alpha\, f\,(-\Delta G^{inject}) \quad \ldots (10)$$

$$\Delta G^{Inject} = E^{dye*} - E_{CB} \quad (11)$$

Where E^{dye*} is the oxidative potential energy in the excited state and E_{CB} represents the reduction potential of the conduction band. E^{dye*} can be estimated by,

Table 3 — The values of HOMO and LUMO energies (E_{HOMO} and E_{LUMO}) and energy gap (E_g) of $Zn_{12}O_{12}$ calculated at B3LYP/6-31G, LANL2DZ and B97D level of theory.

System	Basis set	E_{HOMO} (eV)	E_FeV	E_{LUMO} (eV)	Energy Gap E_g (eV)
$Zn_{12}O_{12}$	B3LYP/6-31G	-6.16	-4.52	-2.89	3.27
$Zn_{12}O_{12}$	B3LYP/LanL2DZ	-5.94	-4.42	-2.79	3.15
$Zn_{12}O_{12}$	B97D	-5.82	-4.27	-2.73	3.09

$$E^{dye*} = E^{dye} - \Delta E \quad \ldots (12)$$

Where E_{dye} represents the energy of oxidation potential in the ground state and ΔE is the energy of electronic vertical transition corresponding to λ_{max}.

3.4 Charge population analysis

Mulliken atomic charge distribution affords the information about the electron population of atoms in the pure $Zn_{12}O_{12}$. The Mulliken charge values were calculated from B3LYP/6-31G, B3LYP/LanL2DZ, and B97D basis sets. The Mulliken atomic charge of individual atoms present in $Zn_{12}O_{12}$ was given in Table 4. For $Zn_{12}O_{12}$ cluster, Zn1, Zn3, Zn5, Zn7, Zn9, Zn11, Zn13, Zn15, Zn17, Zn19, Zn21, and Zn23 atoms have positive charges which are acceptor atoms and the atoms O2, O4, O6, O8, O10, O12, O14, O16, O18, O20, O22 and O24 have negative charges which are donor atoms. The oxygen atom O8 in $Zn_{12}O_{12}$ has a more negative charge which is a donor and a Zinc atom Zn7 has a more positive charge which is an acceptor. The NBO charges of $Zn_{12}O_{12}$ in the singlet ground state are also shown in Table 4. In $Zn_{12}O_{12}$, the charge transfers from the Zn atoms to the O atoms of the material.

3.5 Analysis of Chemical parameters

The ionization potential (I), electron affinity (A), chemical hardness (η), chemical softness (S), the chemical potential (μ), and electrophilicity index (ω) of $Zn_{12}O_{12}$ cluster calculated using B3LYP/6-31G, B3LYP/LanL2DZ and B97D methods were tabulated in Table 5. The global reactivity descriptors are calculated from the energies of HOMO and LUMO in order to study the chemical stability and reactivity of $Zn_{12}O_{12}$.

According to Koopman's theorem[51], the energies of HOMO (E_{HOMO}) and LUMO (E_{LUMO}) are related to the ionization potential (I) and electron affinity (A) as $I = -E_{HOMO}$ and $A = -E_{LUMO}$. The ionization potential of $Zn_{12}O_{12}$ was found to be 6.16 eV. The electron affinity was calculated as 2.89 eV. This calculation correlated with Yadav *et. al.*[52] as the ionization potential (I) is greater than the electron affinity (A). The chemical potential (μ) is defined based on the Equation,

Table 4 — Mulliken atomic charges (Mul) and NBO charges of $Zn_{12}O_{12}$ calculated at B3LYP/6-31G level of theory.

Atoms	$Zn_{12}O_{12\,(Mul)}$	$Zn_{12}O_{12\,(NBO)}$
Zn1	0.905	1.6
O2	-0.817	-1.419
Zn3	0.735	1.503
O4	-0.869	-1.515
Zn5	0.849	1.404
O6	-0.851	-1.524
Zn7	0.964	1.517
O8	-0.875	-1.475
Zn9	0.797	1.469
O10	-0.808	-1.512
Zn11	0.8	1.593
O12	-0.83	-1.392
Zn13	0.898	1.582
O14	-0.845	-1.463
Zn15	0.871	1.499
O16	-0.865	-1.504
Zn17	0.912	1.521
O18	-0.849	-1.494
Zn19	0.923	1.59
O20	-0.853	-1.522

Table 5 — Global Reactivity Descriptors of $Zn_{12}O_{12}$ calculated at B3LYP/6-31G, B3LYP/LanL2DZ and B97D level of theory.

	$Zn_{12}O_{12}$		
Property	B3LYP/6-31G	B3LYP/LanL2DZ	B97D
$I = -E_{HOMO}$ eV	6.16	5.94	5.82
$A = -E_{LUMO}$ eV	2.89	2.79	2.73
$\eta = (I - A)/2$eV	1.63	1.58	1.55
$\mu = -(I + A)/2$eV	-4.52	-4.37	-4.26
$\Psi = -\mu$eV	4.52	4.37	4.26
$S = 1/2\eta$ eV	0.3	0.31	0.32
$\omega = \mu^2/2\eta$eV	6.26	6.04	5.85
Dipole Moment	0.18	0.09	0.12
Polarizability	-92.08	-84.64	-91.05
Hyper Polarizability	3.17	2.79	3.07

$$\mu = -(I+A)/2 \quad \ldots (13)$$

The calculated chemical potential (μ) for $Zn_{12}O_{12}$ was -4.52eV. The Fermi level (E_F) of the cluster is sited at the nuclear point of the energy gap E_g. The chemical potential (μ) is also the central point of the energy gap Eg and hence the Fermi level is similar to

the chemical potential (μ). The electronegativity (Ψ) is the negative of the chemical potential (μ).

The chemical hardness (η) can be calculated as:

$$\eta = (I - A)/2 \quad \ldots (14)$$

The chemical hardness (η) of the $Zn_{12}O_{12}$ cluster was calculated as 1.635 eV. The high value of chemical hardness (η) in $Zn_{12}O_{12}$ predicts its rigid chemical stability. The chemical hardness (η) value depends on the ionization potential (I) and electron affinity (A) values.

The chemical softness (S) and the electrophilicity index (ω) are explained as:

$$S = 1/2\eta \quad \ldots (15)$$

$$\omega = \mu^2/2\eta eV \quad \ldots (16)$$

The chemical softness (S) is the reciprocal of the chemical hardness (η). The chemical softness (S) of $Zn_{12}O_{12}$ was calculated as 0.30 eV. The results of chemical hardness (η) and chemical softness (S) obtained for $Zn_{12}O_{12}$ are same as that of the results obtained for Ali Shokuhi Rad *et al.*[53]**.** The larger the electrophilicity index (ω) of 6.26 eV describes the chemical reactivity of $Zn_{12}O_{12}$. By comparing all the quantum chemical calculations by B3LYP/6-31G, B97D and B3LYP/LanL2DZ, the highest reactivity and stability of $Zn_{12}O_{12}$ were obtained by B3LYP/6-31G level of computation.

3.6 Analysis of NLO parameters

The polarizability and hyperpolarizability are predominant parameters to determine the structural chemistry. The efficiency of the polarizability and hyperpolarizability properties depends on the charge transfer between electron donating and withdrawing groups to study the intramolecular charge transfer. The intermolecular interactions involving the non-bonded type dipole-dipole interactions are determined with the help of the dipole moment of the nanocluster. The stronger the dipole moment, stronger will be the intermolecular interactions. The dipole moment reflects the molecular charge distribution and it is given as a vector in three dimensions. The dipole moment vector is helpful to portray the charge drift over the $Zn_{12}O_{12}$ nanocluster. The inclination of dipole moment vector in $Zn_{12}O_{12}$ be based on the centers of positive and negative charges and its value depends on the possibility of the origin and molecular inclination. The calculated dipole moment for $Zn_{12}O_{12}$ cluster is found as 0.189 Debye. The polarizability and the first order hyperpolarizability have been determined using DFT calculations with B3LYP/6-31G, B3LYP/LanL2DZ and B97D basis sets[54]. The hyperpolarizability can be expressed in terms of x, y, z components as,

$$\mu = (\mu_x^2+\mu_y^2+\mu_z^2)^{1/2} \quad \ldots (17)$$

The total hyper polarizability,

$$\beta_{TOTAL} = (\beta_x^2+\beta_y^2+\beta_z^2)^{1/2} \quad \ldots (18)$$

The mean polarizability,

$$\langle\alpha\rangle = 1/3(\alpha_{xx}+\alpha_{yy}+\alpha_{zz}) \quad \ldots (19)$$

The calculated mean polarizability and hyperpolarizability of $Zn_{12}O_{12}$ were -92.08Debye and 3.17Debye at B3LYP/ 6-31G level of computation.

3.8 Molecular electrostatic potential (MEP)

The electron density of $Zn_{12}O_{12}$ cluster significantly describes the reactivity of electrophilic and nucleophilic sites. The MEP plot displays the cluster size, shape, structure, positive, negative and neutral electrostatic potential regions using colour grading profile. The MEP was simulated using the B3LYP level of the optimized geometry using Gauss view software as shown in Fig. 4. All isosurfaces are depicted with the isovalue of 0.0004e/au3. The blue profile of the positive potential region is around to the electron-rich Zn atoms specify the electrophilic attack while the green profile shows the neutral region. MEP of $Zn_{12}O_{12}$ showed the red region of the negative potential region around oxygen atoms of $Zn_{12}O_{12}$ nanocluster indicating the binding site for nucleophilic attack. This revealed that there was the charge transfer from Zn atoms to O atoms resulting in the ionic bonds present in the $Zn_{12}O_{12}$ nanocluster.

3.9 UV-VIS Spectrum

The UV-Vis absorption spectrum of $Zn_{12}O_{12}$ was analyzed and the wavelength, excitation energies, and

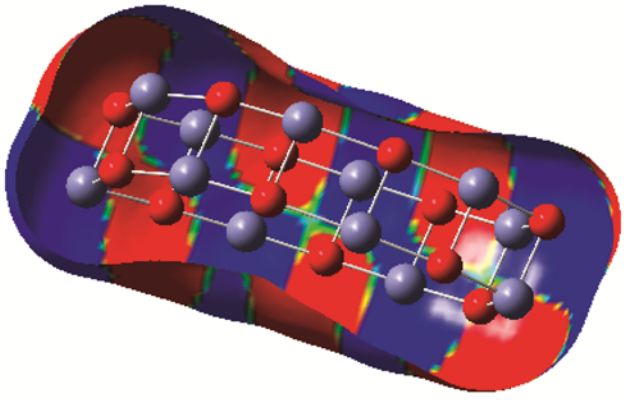

Fig. 4 — The Molecular electrostatic potential of $Zn_{12}O_{12}$ nanocluster

oscillator strength were computed using singlet excited state at TD-DFT with CAM-B3LYP/6-31G functional and CIS method. Calculations by CAM-B3LYP functional predict one intense electronic transition as good agreement with the measured experimental data. The experimental and theoretical absorption wavelength and excitation energies of $Zn_{12}O_{12}$ were shown in Table 6. The high absorption of the $Zn_{12}O_{12}$ cluster was mainly depending on the energy gap. According to the Frank Condon principle, the maximum peak correlates with the vertical excitation.

The electronic excitation observed on $Zn_{12}O_{12}$ was $\pi - \pi^*$ transitions. The energy gap of $Zn_{12}O_{12}$ cluster was 3.27 eV and hence the λ_{max} was fall in the visible region. There are three peaks with excitation energies 4.12, 3.33 and 2.79 eV for $Zn_{12}O_{12}$ observed in TD-DFT calculation with CAM-B3LYP/6-31G level of theory. The excitation wavelengths of the absorption spectrum of $Zn_{12}O_{12}$ were determined as 300, 372 and 444 nm. The high value of oscillator strength has been calculated as 0.076 with the excitation energy of 3.33 eV. This theoretical spectrum is extremely consistent with the experimental UV-VIS spectrum.

UV-Vis absorption spectrum of ZnO nanoparticle recorded in the range 200-800 nm. The experimental UV-VIS spectrum of ZnO at 600 °C with the theoretical UV-Vis spectrum computed at TD-DFT method is shown in Fig. 5. The absorber of the ZnO nanoparticles depends on several factors such as band gap, oxygen deficiency, and surface roughness and impurity centers[55]. Their excitonic absorption maximum peak is observed around 380nm for the ZnO nanoparticles. The spectrum specifies that the material has broad optical absorption window, which is a desired NLO property. The optical energy band gap of ZnO nanoparticles is calculated from classical tauc relation as,

Table 6 — Excitation energy (eV), Oscillator strength (f), excited state transition of $Zn_{12}O_{12}$ nanocluster computed by TD-DFT and CIS method with maximum absorption wavelength of ZnO nano particles calculated by experimental UV-Vis spectrum.

System	Method	Theoretical absorption peak Wavelength (nm)	Oscillator strength (f)	Excitation energy (eV)
$Zn_{12}O_{12}$	TD-DFT	300	0.053	4.12
		372	0.076	3.33
		444	0.005	2.79
$Zn_{12}O_{12}$	CIS	364	0.067	3.4
		412	0.023	3
ZnO	Experiment	380	-	3.2

$$(\alpha h\nu)^2 = A\,(E_g - h\nu)^n \quad \ldots (20)$$

Where h is the Planck's constant, ν is the frequency of vibration, α is the absorption coefficient, Eg is the optical band gap and A is a proportional constant and exponential *n* depends on the transition. The absorption coefficient (α) can be calculated from the spectrum by the relation,

$$\alpha = \{2.3026/t\} \log (1/T) \quad \ldots (21)$$

The value of *n*=1/2, 3/2, 2 and 3 are subjected to the note of electronic transition. The significance of n=1/2 for allowed direct transition, 2 for allowed indirect transition, 3/2 for forbidden direct and 3 for forbidden indirect transition, respectively. Considering a direct band transition in ZnO, a plot between $(\alpha h\nu)^2$ versus photon energy (hν) was drawn for ZnO nanoparticles in Fig. 6. Extrapolation of the

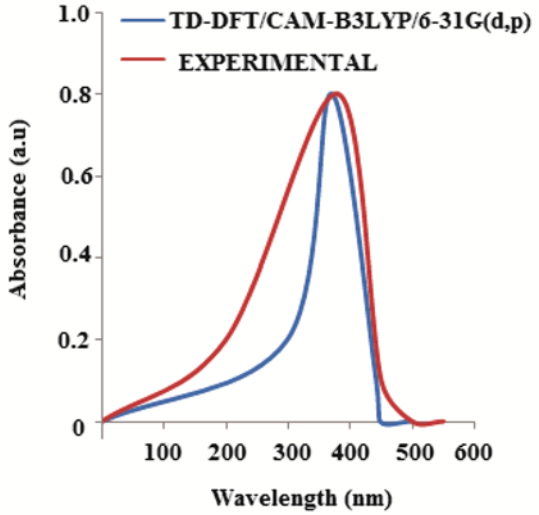

Fig. 5 — The experimental UV-Vis spectrum of ZnO nanoparticles with theoretical UV-Vis spectrum analyzed by excited state computations of TD-DFT method.

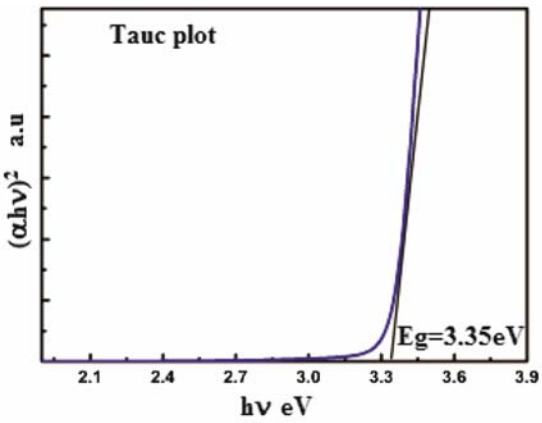

Fig. 6 — The Tauc plot of ZnO nanoparticles.

linear region of this plot gives direct energy band gap of 3.3 eV. This is also in good agreement to the DFT computed energy gap.

3.10 Surface Morphology by FESEM with EDAX analysis

The surface morphology and topography of ZnO nanoparticles was examined by Field emission scanning electron microscopy (FESEM) results. Figure 7 shows the FESEM image of synthesized ZnO nanoparticles. From the Fig. 6, we can find that the ZnO nanoparticles form a hexagon-like structure and this surface morphology is consistent with the theoretical optimal profile of $Zn_{12}O_{12}$ cluster. The mean grain size of ZnO was determined as 129 nm and it is in good agreement with the XRD results at 800 °C. The surface elements of ZnO were determined by energy-dispersive X-ray spectroscopy (EDAX). EDAX analysis confirms that the Zn and O atoms are present in the ZnO nanoparticle. The EDAX image was shown in Fig. 8. The amount of transition metal ions present in the ZnO nanoparticles are observed. In the ZnO nanoparticles, the composition of Zn and O atom was found to be Zn=48.86% and O=51.14%, respectively.

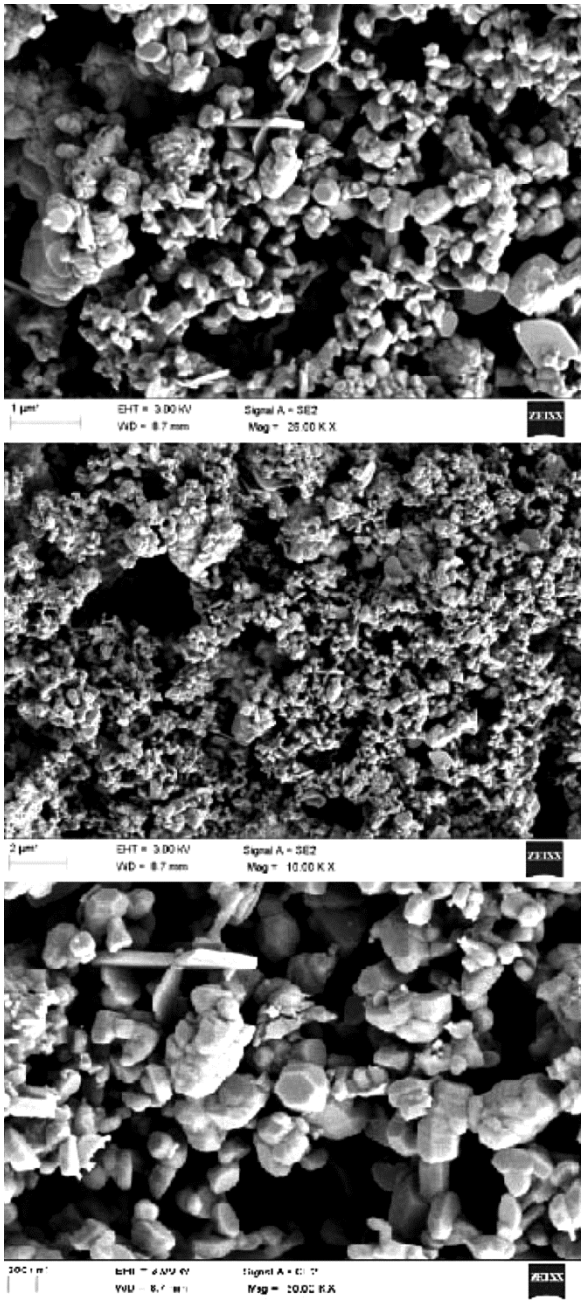

Fig. 7 — The FESEM image of green synthesized ZnO nanoparticles.

3.11 Vibrational assignments

The vibration frequencies are the unique parameter to explore the local minimum in structures. Transmittance is the principal features of Zn-O vibration[56]. The simulated IR spectrum of $Zn_{12}O_{12}$ shows the peaks at 430cm^{-1}, 451cm^{-1} and 547cm^{-1} have corresponded to the Zn-O stretching vibrations computed as B3LYP/6-31G level of geometry. In green synthesized ZnO nanoparticles, Zn-O is stretching was observed at 457 cm^{-1} and 545 cm^{-1}. The calculated peaks found at 451 cm^{-1} and 547cm^{-1} showing a better agreement with the experimental values. The synthesized ZnO nanoparticle showed approximate similar IR bands of $Zn_{12}O_{12}$ nanocluster that are seen in Fig. 9. Experimental and calculated vibrational frequencies in cm^{-1} for ZnO nanomaterial are listed in Table 7.

3.12 Natural Bond Orbital (NBO) analysis

The NBO calculated hybridizations are of great significance parameters for structure analysis. It was determined using the Gaussian 09 package at the B3LYP/6-31G (d,p) method. Natural Bond Orbital's are localized few-center orbital explain the Lewis-like

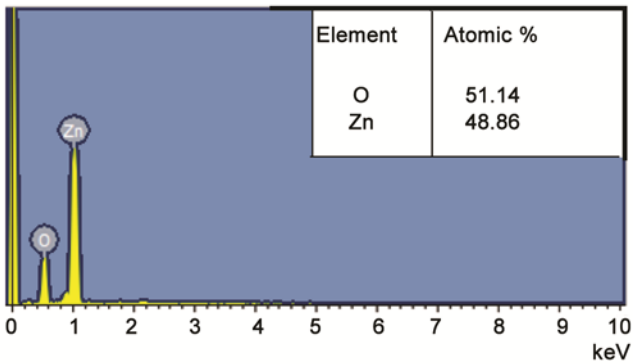

Fig. 8 — The EDAX spectra of ZnO nanoparticles.

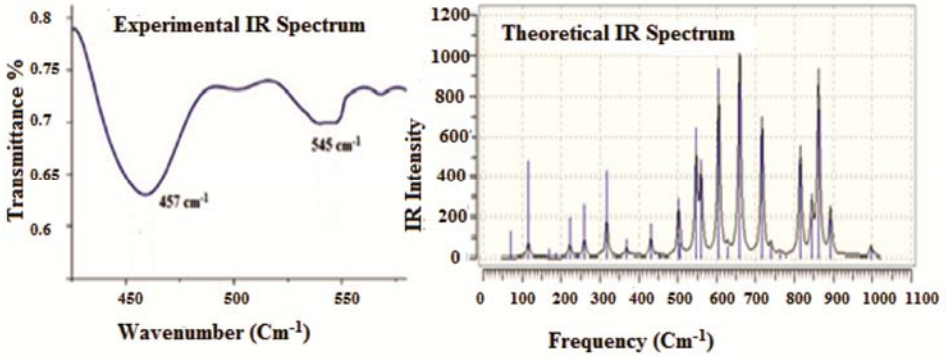

Fig. 9 — The simulated IR and experimental IR spectrum of ZnO nanoparticles

Table 7 — Experimental FT-IR and calculated vibrational frequencies in cm^{-1} for ZnO nanomaterial.

Experimental ZnO	Calculated B3LYP-$Zn_{12}O_{12}$	vibrational Assignment
457	451	Zn-O stretching
545	547	Zn-O stretching

molecular bonding pattern in the compact form of electron pairs.

NBOs are localized "maximum occupancy" orbital whose leading N/2 members (or N members in the open-shell case) and Lewis-like description of the total N-electron-density. Second-order perturbation theory indicates that all possible interactions are analyzed between "filled" (donor) Lewis-type NBOs and "empty" (acceptor) non-Lewis NBOs. Evaluation of NBO analysis helps to investigate the interaction between donor (i) level bonds donor-acceptor (j) level bands. The result of the interaction is a loss of occupancy from the concentration of electron NBO of the idealized Lewis structure into an empty non-Lewis orbital[57,58]. For each donor (i) and acceptor (j) the stabilization energy E(2) concerned with the delocalization i → j is as follows:

$$E(2) = \otimes Eij = qi(Fij)^2/(Ej-Ei)E(2) = \Delta Eij = qi(Fij)^2/(Ej-Ei) \quad \ldots (22)$$

Where qi is the donor orbital occupancy, Ei and Ej are the diagonal elements and Fij is the of diagonal NBO Fock matrix element. The NBO atomic charge transfer energy related to the electron donating from the π (Zn3-O4) to the acceptor antibonding π* (Zn3-O4) (Zn3-O24) orbital energies are 21.98, 15.29 kcal/mol results the strongest stabilization energy. Similarly, the interaction between the LP(1) O16, LP(3) O24 to the antibonding acceptor π* (Zn1-O16), (Zn3-O4) and their energies are 15.27, 12.18 Kcal/Mol. The large E(2) value exhibits the intensive interaction between electron-donors and electron-acceptors and the second order perturbation theory analysis of Fock matrix in NBO basis of $Zn_{12}O_{12}$ nanocluster are given in Table 8. Stabilization of the system was observed of the following strong

Table 8 — Second order perturbation theory analysis of Fock matrix in NBO basis of $Zn_{12}O_{12}$ nanocluster .

Donor (i)	Type	Acceptor (j)	Type	E(2)[a]	E(j)_E(i)[b]	F(i,j)[c]
Zn1-O16	π	Zn3-O4	π*	4.95	0.93	0.061
Zn1-O16	π	Zn3-O24	π*	1.13	0.72	0.026
Zn3-O4	π	Zn3-O16	π*	5.51	0.75	0.057
Zn3-O4	π	Zn3-O24	π*	5.55	0.76	0.058
Zn3-O16	π	Zn1-O16	π*	4.09	0.54	0.043
Zn3-O16	π	Zn3-O4	π*	21.98	0.98	0.131
Zn3-O16	π	Zn3-O24	π*	15.29	0.77	0.097
Zn3-O24	π	Zn3-O4	π*	4.9	0.94	0.061
Zn3-O24	π	Zn3-O16	π*	3.68	0.72	0.046
Zn3-O24	π	Zn3-O24	π*	1.41	0.73	0.029
LP(5) Zn1	n	Zn3-O16	π*	0.75	0.96	0.024
LP(5) Zn3	n	Zn3-O24	π*	0.62	0.94	0.022
LP(1) O4	n	Zn3-O4	π*	1.61	1.3	0.041
LP(1) O4	n	Zn3-O16	π*	2.2	1.08	0.044
LP(1) O4	n	Zn3-O24	π*	1.71	1.09	0.039
LP(2) O4	n	Zn3-O4	π*	5.51	1.39	0.078
LP(2) O4	n	Zn3-O16	π*	4.36	1.17	0.064
LP(2) O4	n	Zn3-O24	π*	3.7	1.19	0.059
LP(1) O16	n	Zn1-O16	π*	15.27	0.98	0.112
LP(1) O16	n	Zn3-O4	π*	3.37	1.41	0.062
LP(1) O16	n	Zn3-O16	π*	1.36	1.119	0.036
LP(1) O16	n	Zn3-O24	π*	3.28	1.21	0.057
LP(2) O16	n	Zn1-O16	π*	12.71	0.79	0.091
LP(2) O16	n	Zn3-O4	π*	4.16	1.22	0.064
LP(2) O16	n	Zn3-O16	π*	1.81	1	0.038
LP(2) O16	n	Zn3-O24	π*	1.06	1.02	0.032
LP(1) O24	n	Zn3-O4	π*	8.37	1.4	0.097
LP(1) O25	n	Zn3-O16	π*	4.29	1.18	0.064
LP(1) O26	n	Zn3-O24	π*	10.42	1.19	0.1
LP(3) O24	n	Zn3-O4	π*	12.18	0.92	0.097
LP(3) O24	n	Zn3-O16	π*	4.98	0.7	0.055
LP(3) O24	n	Zn3-O24	π*	7.23	0.71	0.066

intramolecular hyper conjugative interactions causing increased electron density (ED) and intramolecular charge transfer (ICT)[59].

4 Conclusion

The synthesis of ZnO nanoparticles using *Mangifera indica* through green chemistry approach with several advantages like economical, efficient, eco-friendly, energy efficient and cost-effectively provide a vast potential for their use in biomedical applications. We have reported the experimental study of ZnO nanoparticles and quantum chemical calculations of $Zn_{12}O_{12}$ through DFT/TD-DFT computations. The XRD predictions indicated that the green synthesized ZnO nanoparticles had a wurtzite structure. The optical band gap calculated from UV-Vis spectroscopy results ZnO nanoparticle absorb in the UV-Vis range. The FESEM image shows the spherical, cauliflower and irregular cluster morphologies. The structural parameters from XRD analysis was compatible with the frontier orbital analysis and optimized geometry of theoretical predictions. It is concluded that the lowest singlet excited state of the nanoparticle is mainly derived from the HOMO-LUMO (π- π^*) electronic transition. Information on the charge density distribution and site of chemical activity of the nanoparticle has been obtained by reactivity descriptors and MEP surface. Comparison of theoretical and experimental data exhibits good correlations confirming the reliability of the quantum chemical method to reveal the reactivity of the ZnO nanomaterial. The green synthesized ZnO nanoparticles provide healthier workplaces and communities leading to lessening waste and safer products. The green synthesis technique provides an easy and quick access to ZnO nanoparticles displaying greater interest for technological applications specifically for biomedical.

References

1 Naseem S M, Ahmed A & Tripathi P, *Optik*, 185 (2019) 599.
2 Mackowski S, Karczewski G, Wojtowicz, Qju X, Howe J Y, Mayer H M, Tuncer E & Parantharaman M P, *Appl Surf Sci*, 257 (2011) 4057.
3 Dheivamalar S & Bansura B K, *Orient J Chem*, 34 (2018) 5.
4 Duan J, Huang X & Wang E, *Mater Lett*, 60 (2006) 1918.
5 Aslanzadeh S, *J Mol Model*, 22 (2016) 160.
6 Abdulsattar M A, *J Mol Model*, 23 (2017) 125.
7 Sheng L, Gang L, Zhang W & Wang K, *Optik*, 184 (2019) 90.
8 Nakahara K, Takasu H, Fons P, Yamada A, Matsubara K, Hunger R & Niki S, *Appl Phys Lett*, 79 (2001) 4139.
9 Wang Z S, Huang C H, Huang Y Y, Hou Y J, Xie P H, Zhang B W & Cheng H M, *Chem Mater*, 13 (2001) 678.
10 Xu J Q, Pan Q Y, Shun Y A & Tian Z Z, *Sens Actuators B Chem*, 66 (2000) 277.
11 Sahu D R, Lin S Y & Huang J L, *Sol Energy Mater Sol Cells*, 91 (2007) 851.
12 Wang Z L & Song J H, *Science*, 14 (2006) 242.
13 Behran E C, Foehrweiser R K, Myers J R, French B F & Zandler M E, *Phys Rev A*, 49 (1994) R1543.
14 Malloci G, Chiodo L, Rubio A & Mattoni A, *J Phys Chem C*, 116 (2012) 8741.
15 Masuda Y, Yamagishi M, Seo W S & Koumoto K, *Crystal Growth Design*, 8 (2008) 1503.
16 Tokumoto M S, Pulcinelli S H, Santilli C V & Briois V, *J Phys Chem*, 107 (2003) 568.
17 Zhang H, Yang D, Ji Y, Ma X Y, Xu J & Que D L, *J Phys Chem B*, 18 (2004) 3955.
18 Hu X L, Zhu Y J & Wang SW, *Mater Chem Phys*, 88 (2004) 421.
19 Singhal M, Chhabra V, Kang P & Shah D O, *Mater Res Bull*, 32 (1997) 239.
20 Wu J J & Liu S C, *Adv Mater*, 14 (2002) 215.
21 Zhang Z, Yu H, Shao X & Han M, *Chem Eur J*, 11 (2005) 3149.
22 Kim J H, Choi W C, Kim H Y, Kang Y Y & Park K, *Powder Technol*, 153 (2005) 166.
23 Wang J M & Gao L, *Inorg Chem Commun*, 6 (2003) 877.
24 Tsuzuki T & McCormick P G, *Scripta Mater*, 44 (2001) 1731.
25 Okuyama K & Lenggoro I W, *Chem Eng Sci*, 58 (2003) 537.
26 Rataboul F, Nayral C, Casanove M J, Maisonnat A & Chaudret B, *J Organomet Chem*, 643 (2002) 307.
27 Sato T, Tanigaki T, Suzuki H, Saito Y, Kido O, Kimara Y & Kaito C, *J Cryst Growth*, 255 (2003) 313.
28 Yanrong L, Xueming Z, Yuna X, Junchen L, Shiting W & Hongze Z, *Optik*, 180 (2019) 151.
29 Sarsar V, Selwal K K & Selwal M K, *J Microbiology Biotechnol Res*, 3 (2013) 27.
30 Philip D, *Spectrochim Acta A; Mol Biomol Spectr*, 77 (2010) 807.
31 Kumar R S, Kumar S V, Ramaiah A, Agarwal H, Lakshmi T & Roopan S, *Enzym Microbial Technol*, 117 (2018) 91.
32 Dola S, Kumar V T & Subba R P S, *Prog Biomater*, 6 (2017) 57.
33 Frisch M J, Trucks G W, Schlegel H B, Scuseria G E, Robb M A, Cheeseman J R, Scalmani G, Barone V, Mennucci B, Peterson G A, Nakatsuji H, Caricato M, Li X, Hratchian H P, Izmaylov A F, Bloino J, Zheng G, Sonnenberg J L, Hada M, Ehara M, Toyota K, Fukuda R, Hasegawa J, Ishida M, Nakajima T, Honda Y, Kitao O, Nakai H, Vreven T, Montgomery J A, Jr, Peralta J E, Ogliaro F, Bearpark M, Heyd J J, Brothers E, Kudin K N, Staroverov V N, Kobayashi R, Normand J, Raghavachari K, Rendell A, Burant J C, IyengaSr S S, Tomasi J, Cossi M, Rega N, Millam M J, Klene M, Knox J E, Cross J B, Bakken V, Adamo C, Jaramillo J, Gomperts R, Stratmann R E, Yazyev O, Austin A J, Cammi R, Pomeli C, Ochterski J W, Martin R L, Morokuma K, Zakrzewski C G, Voth G A, Salvador P, Dannenberg J J, Dapprich S, Daniels A D, Farkas O, Foresman J B, Ortiz J V, Cioslowski J & Fox D J, Gaussian 09, Revision D.01, Gaussian, Inc Wallingford CT, (2009).
34 Lee C, Yang W & Parr R G, *Phys Rev B, 37* (1988) 785.

35 O'Boyle N M, Tenderholt A L & Langner K M, *J Comput Chem*, 9 (2008) 839.
36 Ochterski J W, Thermochemistry in Gaussian Inc, Pittsburgh, PA, (2000).
37 Ali S R & Khurshid A, *J Alloys Comp*, 678 (2016) 317.
38 Fatemeh F, Milad N & Sara S G, *Appl Surf Sci*, 366 (2016) 545.
39 Birajdar S D, Khirade P P, Bhagwat V, Humbe A V & Jadhav K, *J Alloys Compd*, 683 (2016) 513.
40 Seetawan U, Jugsujinda S, Seetawan T, Ratchasin A, Euvananont C, Junin C, Thanachayanont C & Chainaronk P, *Mater Sci Appl*, 2 (2011) 1302.
41 Wang Z L, *Mater Today*, 7 (2004) 26.
42 Hossain M F, Zhang Z H & Takahashi T, *Nano-Micro Lett*, 2 (2010) 53.
43 Noh Y J, Na S I & Kim S S, *Sol Energ Mat Sol Cells*, 117 (2013) 139.
44 Bacaksiz E, Aksu S, Yılmaz S, Parlak M & Altunbas M, *Thin Solid Films*, 518 (2010) 4076.
45 Yilmaz S, Bacaksiz E, McGlynn E, Polat I & Qzcan S, *Thin Solid Films*, 520 (2012) 5172.
46 Maniv S & Zangvil A, *J Appl Phys*, 47 (1978) 2787.
47 Wang X S, Wu Z C, Webb J F & Liu Z G, *Appl Phys A*, 77 (2003) 561.
48 Warren B E, X-ray diffraction, Dover, New-York (1990) 253.
49 Aksoy S, Caglar Y, Ilican S & Caglar M, *Adv Control Chem Eng Civ Eng Mech Eng*, (2010) 227.
50 Dheivamalar S & Bansura B K, *Indian J Pure Appl Phys*, 57 (2019) 713.
51 Koopmans T, *Physica*, 1 (1933) 104.
52 Yadav P S & Pandey D K, *Appl Nanosci*, 2 (2012) 351.
53 Ali S R & Khurshid A, *Thin Solid Films*, 612 (2016) 179.
54 Dheivamalar S & Bansura B K, *Heliyon*, 5 (2019) e02903.
55 Gaussview 4.1.2, Gaussian Inc, Wallingford, CT, (2004).
56 Fogarasi G, Zhov X, Taylor P W & Pulay P, *J Am Chem Soc*, 114 (1992) 8191.
57 Agarwal D C, *Nucl Instrum Methods Phys Res*, 244 (2006) 136.
58 Glendening E D, Reed A E, Carpenter J E & Weinhold F, NBO Version 3.1, TCI, University of Wisconsin: Madison, (1998).
59 Reed A E, Curtiss L A & Weinhold F, *Chem Rev*, 88 (1988) 899.